Rapid Communications

Microscopic theory of onset of decaging and bond-breaking activated dynamics in ultradense fluids with strong short-range attractions

Ashesh Ghosh [1,2] and Kenneth S. Schweizer [1,2,3,4,*]

[1] *Department of Chemistry, University of Illinois at Urbana-Champaign, Illinois 61801, USA*
[2] *Materials Research Laboratory, University of Illinois at Urbana-Champaign, Illinois 61801, USA*
[3] *Department of Material Science, University of Illinois at Urbana-Champaign, Illinois 61801, USA*
[4] *Department of Chemical & Biomolecular Engineering, University of Illinois at Urbana-Champaign, Illinois 61801, USA*

(Received 14 March 2020; accepted 4 June 2020; published 19 June 2020)

We theoretically study thermally activated "in cage" elementary dynamical processes that precede full structural relaxation in ultradense particle liquids interacting via strong short-range attractive forces. The analysis is based on a microscopic theory formulated at the particle trajectory level built on the dynamic free energy concept and an explicit treatment of how attractive forces control the formation and lifetime of physical bonds. Mean time scales for bond breaking, the early stage of cage escape, and non-Fickian displacement by a fixed amount are analyzed in the repulsive glass, bonded repulsive (attractive) glass, fluid, and dense gel regimes. The theory predicts a strong length-scale-dependent growth of these time scales with attractive force strength at fixed packing fraction, a much weaker slowing down with density at fixed attraction strength, and a strong decoupling of the shorter bond-breaking time with the other two time scales that are controlled mainly by perturbed steric caging. All results are in good accord with simulations, and additional testable predictions are made. The classic statistical mechanical projection approximation of replacing all bare attractive and repulsive forces with a single effective force determined by pair structure incurs major errors for describing processes associated with thermally activated escape from transiently localized states.

DOI: 10.1103/PhysRevE.101.060601

Introduction. How strong short-range attractive forces control *length-scale-dependent* slow dynamics and kinetic arrest of soft matter systems is a problem of broad fundamental interest which continues to challenge theoretical understanding. The central issue is the nonadditive interplay of physical bonding and steric caging in ultrahigh density fluids and colloidal suspensions in determining *activated* relaxation, viscoelasticity, intermediate time non-Fickian motion, diffusion, and nonlinear rheology [1–9].

Seminal studies based on microscopic ideal mode coupling theory (MCT) predicted a subtle structure-induced competition between the dynamical consequences of repulsive force caging and physical bonding, and led to the concepts of attractive (bonded) glasses and re-entrant glass melting [3,8–10]. However, MCT does not account for ergodicity restoring activated processes, resulting in bonds and cages that persist forever and qualitative disagreements with simulation and experiment [6,11–13]. The nonlinear Langevin equation (NLE) theory [14,15] and its more recent Elastically Collective NLE (ECNLE) extension [16] explicitly address activated motion by avoiding closure approximations for ensemble-averaged time correlation functions in favor of a stochastic trajectory level description. The central quantity is the "dynamic free energy" [15]. Long time structural relaxation occurs via thermal noise driven barrier hopping, and ECNLE theory predictions are in good accord with activated relaxation in *repulsion*-dominated colloidal [16,17], molecular [16,18], and polymeric [19,20] glass forming liquids. Dynamic constraints are quantified based on the classic "projection approximation" [10] that replaces all Newtonian forces with an effective force determined by the equilibrium pair correlation function.

Very recently we established that use of the projection approximation for very dense strongly attractive particle fluids that can form long-lived physical bonds results in *qualitatively* incorrect predictions for *long time activated* relaxation in the ECNLE theoretical framework [21]. A modified approach [projectionless dynamics theory (PDT) [21,22]] for quantifying effective forces was formulated which explicitly treats how bare short-range attractive *forces* create physical bonds, control their lifetime, and interfere with steric caging. Detailed comparisons with experiments and simulations suggest it properly captures re-entrant dynamic arrest, strong nonmonotonic variation of the *activated* structural relaxation time and long time diffusion constant with attraction strength, and *kinetic* criteria for glass and gel formation based on a practical observation time [21]. The approach is conceptually distinct from attempts [8,9,23,24] to use ideal MCT to rationalize slow activated dynamics in dense attractive colloids.

The ECNLE-PDT approach has only considered the slowest structural relaxation process associated with large amplitude hopping and barrier crossing for which longer range collective elasticity effects are crucial [21,22]. Since the theory is formulated in terms of a spatially resolved dynamic free energy [14,15], earlier time thermal fluctuation driven

*kschweiz@illinois.edu

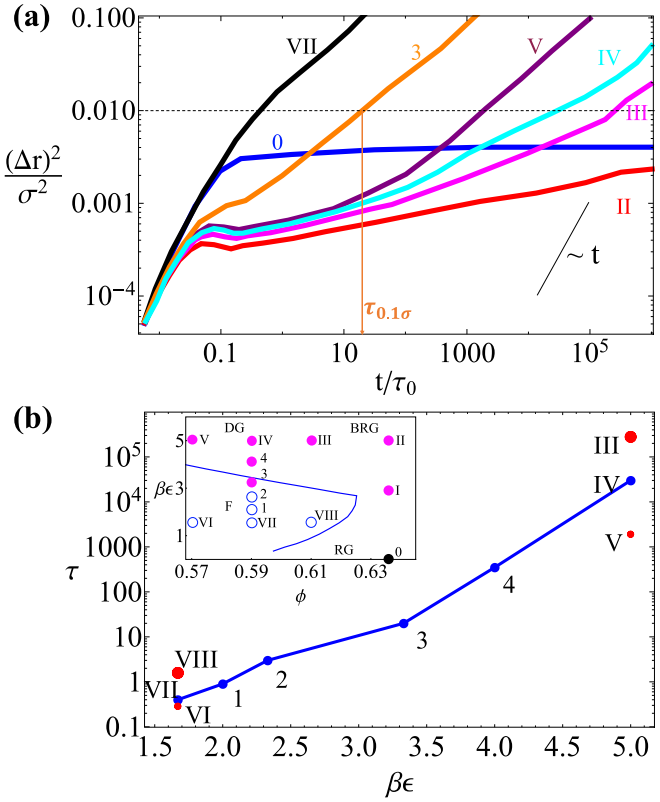

FIG. 1. (a) Simulation MSD [6] data for selected state points as labeled in the inset of (b). Panel (b) is the time required (in dimensionless simulation units) for the MSD to reach $0.01\sigma^2$ (horizontal black dashed line in (a), illustrated for state 3 by the orange vertical arrow) which is plotted as a function of dimensionless attraction strength. Simulations of the filled (open) state points do not (do) reach the long time Fickian behavior.

"uphill" motions on smaller length scales can also be addressed. However, such "in-cage" activated motions are *not* expected to be strongly influenced by collective elastic effects, and the need to account explicitly for attractive forces for such motions is a priori unclear. This Rapid Communication reports a microscopic theory for these processes which incisively tests both the concept of a dynamic free energy and the importance of a direct treatment of attractive forces for in-cage motion. Our work also serves as a theoretical basis for understanding the large scale simulations (over eight decades in time) of Zaccarelli and Poon (ZP) [6] where repulsive glass (RG), bonded repulsive glass (BRG) or attractive glass (AG), and dense gel (DG) regimes of slow dynamics exist. The absolute and relative time scales for the onset of decaging and bond breaking and how they evolve with density and attractive force strength and range are analyzed. These phenomena occur well beyond the ideal MCT transition in a regime of activated, highly non-Gaussian motion.

Simulation background. ZP simulated a binary mixture of hard spheres that interact via a short-range (3% mean particle diameter) square well attraction of strength $\epsilon = 0 - 5k_BT$ at very high mixture total packing fractions of $\phi = 0.57{-}0.63$. The inset of Fig. 1(b) shows the specific state points studied, along with an empirically shifted ideal MCT kinetic arrest boundary [25]. The attraction strengths span the range from well below to well above the re-entrant "nose" feature (a dynamic crossover in ECNLE theory) associated with nonmonotonic or re-entrant dynamics [3,6,8,25]. Figure 1(a) shows selected single particle mean square displacement (MSD) data [6] which are mostly subdiffusive over the time scales probed and involve displacements well below a particle diameter. The densest RG state 0 is a hard sphere (HS) glass where cages are stable (flat MSD) on the simulation time scale. BRG states I (not shown) and II exhibit a temporal trapping on the attraction range scale due to bond formation, followed by a slow increase towards the hard sphere fluid long-lived plateau. States III–V are strongly attractive but at modestly lower packing fractions (DG) and show similar, but slightly weaker, short time dynamic localization and no saturation of the MSD after the bond-breaking event. Weaker attractive states VI, VII (plotted), and VIII, deemed "fluids" (F) in [6], show an inflection point in the MSD before crossing over to Fickian diffusion. The form of the MSD appears to continuously evolve with attraction strength and packing fraction, with the RG, BRG, DG, and F states all exhibiting intermittent dynamics.

A specific "bonding" time correlation function [6] was also computed which quantifies the number of particles within a bonding distance $\sigma + a$ of a tagged particle, where "a" is the attraction range. A "decaging" time was also studied, defined as the mean time for a particle to displace a distance $\sigma + R^*$, where R^* is the MSD *inflection* point of the corresponding *pure* HS fluid (a *fixed length* scale criterion). The length scale R^* signals a temporal crossover to the *early* stages of cage escape which occurs for a displacement far below that associated with the barrier hopping event that underlies structural relaxation. An overarching conclusion was the bond-breaking time is always (much) shorter than the decaging time (a form of "decoupling"), and caging dominates longer time dynamics in attractive glasses (BRG). With increasing packing fraction and/or attraction strength, the difference between these two time scales, and hence degree of decoupling, grows. A computational limitation was bond lifetimes of only a few simulated states were determined, but it was found to modestly (of order a decade) increase both with packing fraction at high attraction strength (DG $\rightarrow$ BRG), and at very high density as attraction strength grows (RG $\rightarrow$ BRG).

For the purpose of testing our theoretical analysis against simulation over a wide parameter space, we define a characteristic time for in-cage motion, $\tau_{0.1\sigma}$, from the MSD data as $\langle r^2(t = \tau_{0.1\sigma})\rangle = 0.01\sigma^2$ [black dashed line in Fig. 1(a)]. This corresponds to the average time for a particle to move a relatively short distance (0.1σ). Our logic for this choice is that it corresponds to a displacement *well beyond* a vibrational or bonding distance scale, and thus reflects the combined consequences of bond breaking and the early stage of decaging. It is also sufficiently beyond the narrow transient bonding plateau of the MSD to allow unambiguous extraction of a time scale from the simulations, characteristic of in-cage dynamics over a wide parameter range. In principle, we can theoretically analyze the mean time for other choices of the characteristic MSD, which will continuously decrease with a shorter length-scale criterion.

TABLE I. Comparison of simulation results [6] for the overall range of variation of $\tau_{0.1\sigma}$ along different trajectories in Fig. 1 with the corresponding hybrid PDT ECNLE theory predictions for a monodisperse sphere model with an exponential attraction of 3% range. Ratios for simulation (theory) correspond to the state point mentioned under trajectory.

Trajectory		Ratio of time scales $\tau_{0.1\sigma}$	
Simulation state in Fig. 1(b)	Theory state $= (\phi, \beta\epsilon)$	Simulation	Theory
VI → V	(0.56, 0.55) → (0.56, 1.65)	6.7×10^3	4.4×10^3
VII → IV	(0.58, 0.55) → (0.58, 1.65)	7.5×10^4	2.6×10^4
VIII → III	(0.60, 0.55) → (0.60, 1.65)	2×10^5	5.4×10^5
VI → VIII	(0.56, 0.55) → (0.60, 0.55)	5×10^0	5.1×10^0
V → III	(0.56, 1.65) → (0.60, 1.65)	1.5×10^2	6×10^2

From the simulation MSD data [6] we determined $\tau_{0.1\sigma}$ associated with five trajectories in the dynamic map of Fig. 1(b). For the vertical trajectories VI → V, VII → IV, VIII → III, we find this time scale *massively* varies with increasing attraction strength by factors of ∼6700, 75 000, and 200 000, respectively, growing for higher packing fractions. In strong contrast, the horizontal trajectories V → III and VI → VIII vary by factors of only ∼5 and 150, respectively. The time scales are plotted in Fig. 1(b) as a function of attraction strength. The vertical trajectory data can be roughly fit to an Arrhenius form in attraction energy: $\tau_{0.1\sigma}(\beta\epsilon) = \tau_{0.1\sigma}(\beta\epsilon = 1.67) \times e^{\alpha(\phi)(\beta\epsilon - 1.67)}$. The effective activation energy is packing fraction dependent via $\alpha(\phi)$ which we find to be $(VI \to V) \approx 2.64$, $\alpha(VII \to IV) \approx 3.37$, $\alpha(VIII \to III) \approx 3.62$. Thus, effective barriers are well beyond a single bond energy and increase with density, trends which indicate the importance of many body effects and coupling of bonding and caging constraints. Figure 1 and Table I establish that changing attraction strength at fixed packing fraction produces *much* stronger changes of dynamics than vice versa.

The simulation findings can provide incisive tests of two important questions: (i) Does the dynamic free energy concept faithfully capture the bond-breaking and decaging time scales over a wide parameter space (both ϕ and $\beta\epsilon$)? (ii) Does the *qualitative* difference for the structural relaxation time predicted based on the explicit treatment of attractive forces (and its enormous established superiority) [21] persist for smaller time or length scale "in cage" activated motion? We believe this second question is of broad interest, and the answer is not obvious since collective elasticity is unimportant for in-cage dynamics in qualitative contrast to its dominant role for barrier crossing and full structural relaxation [21].

Model and theory. We consider [21] the simplest monodisperse sticky hard-sphere model: A fluid of packing fraction $\phi = \frac{\pi}{6}\rho\sigma^3$, where ρ is number density and σ the particle diameter, with particles attracting via an exponential pair potential, $\beta v(r) = -\beta\epsilon e^{-(r-\sigma)/a}$ for $r \geqslant \sigma$, $\beta\epsilon > 0$. Equilibrium pair correlation functions are computed using the Ornstein-Zernike theory with the Percus-Yevick closure [26]. Trajectories are quantified by the angularly averaged scalar

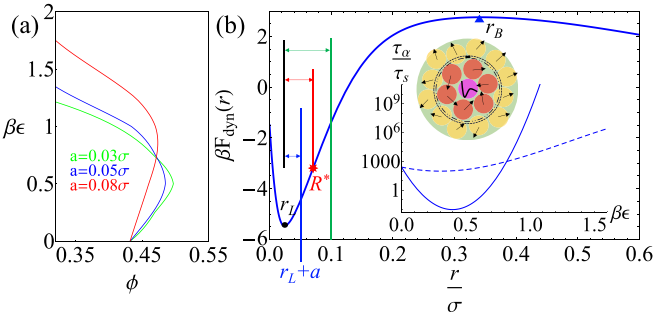

FIG. 2. (a) Ideal (naïve MCT) kinetic arrest map based on the hybrid PDT effective force approximation [21] for three short attraction ranges. (b) Example dynamic free energy as a function of particle displacement for the $\phi = 0.58$ hard-sphere fluid. Inset: mean alpha relaxation time for $\phi = 0.58$ and $a = 0.03\sigma$ as a function of attraction strength for the projected (dashed) and hybrid-PDT (solid) effective force approximations. Also shown is a schematic of the conceptual basis of ECNLE theory which involves cage scale activated motion coupled with a longer range elastic fluctuation outside the cage.

displacement of a tagged spherical particle under the influence of a dynamic free energy $F_{\rm dyn}(r)$, the gradient of which describes the effective force on a tagged particle due to its surroundings [15]:

$$\frac{F_{\rm dyn}(r)}{k_BT} = -3\ln\left(\frac{r}{\sigma}\right) - \rho\int\frac{d\vec{k}}{(2\pi)^3} \times \frac{|\vec{M}(k)|^2 S(k)}{k^2[1+S^{-1}(k)]} e^{-(k^2r^2/6)[1+S^{-1}(k)]}, \quad (1)$$

where $S(k) = [1 - \rho C(k)]^{-1}$ is the static structure factor, $C(k)$ is the direct correlation function, and $M(k)$ is the Fourier transform of the *effective* interparticle force. In the standard projected force approximation [14,15] $|\vec{M}_{\rm MCT}(k)| = kC(k)$, and attractive forces enter *only* via their effect on equilibrium structure. In contrast, in our hybrid-PDT approach, attractions modify structure *plus* enter in an explicitly dynamical manner via the attractive *force* [21],

$$\vec{M}_{\rm hybrid}(k) = kC_0(k)\hat{k} + \int d\vec{r}g(r)\vec{f}_{\rm att}(r)e^{-i\vec{k}\cdot\vec{r}}, \quad (2)$$

where the subscript 0 indicates the pure hard sphere fluid quantity. Moreover, there are cross correlations or interference between caging and bonding dynamical effects in the hybrid PDT approach which were shown to be of qualitative importance for structural relaxation [21].

Beyond the naïve (single particle) MCT transition (in reality a crossover) the dynamic free energy has a (transient) localization length at $r = r_L$ and a barrier of height F_B at $r = r_B$ [Fig. 2(b)]. ECNLE theory includes longer range collective elastic fluctuations as a critical component of the alpha relaxation event [16,17] because a relatively large "jump distance" is required to reach the barrier. The latter incurs a significant collective elastic energy cost in the medium outside the cage region (see [21,22] and the Supplemental Material (SM) [27]). However, the same ideas apply for any smaller length scale "uphill" motion from $r = r_L$ to $r = x$ corresponding to the displacement $\Delta r_x = x - r_L$. As physically expected, we have

numerically verified that longer range elasticity effects are *negligible* for the much smaller length scale bond-breaking and decaging events. Hence, the time scale of these activated processes is determined entirely by in-cage physics via the dynamic free energy. Thus, the mean time required for particles to displace from $r = r_L$ to $r = x$ is then calculated from Kramers theory as [15]

$$\frac{\tau_x}{\tau_s} = \sigma^{-2} \int_{r_L}^{x} e^{\beta F_{\rm dyn}(z)} dz \int_{r_L}^{z} e^{-\beta F_{\rm dyn}(y)} dy \qquad (3)$$

where $\tau_s = \beta \zeta_s \sigma^2$ is the known [17] short time scale, here taken as the elementary unit of time.

We note that the hybrid PDT-ECNLE theory has been very recently employed [21] to study aspects of the non-Gaussian parameter for dense attractive particle fluids including its peak amplitude and corresponding time (t^*) which occur at a mean particle displacement (R^*) associated with the location of the maximum restoring force of the dynamic free energy [28,29] [Fig. 2(b)]; good agreement with simulation was demonstrated [30]. Importantly, it has been shown that R^* is coincident with the inflection point of the MSD(t) [28,29]. This is physically intuitive since maximal deviation from Gaussian or Fickian motion is expected to occur when the cage restoring force is largest, thereby correlating R^* directly with the MSD inflection point. Hence, we can compute a decaging time of clear physical meaning (and compare with the ZP simulations [6]) from the mean time to displace a distance R^*.

Results and comparison to simulation. As relevant background, Fig. 2(a) shows naïve MCT localization boundaries based on the hybrid PDT effective force formulation. Figure 2(b) shows an example dynamic free energy well beyond the naïve MCT crossover for the hard sphere fluid at $\phi = 0.58$, and the four relevant length scales are indicated. The inset plots the structural relaxation time as a function of attraction strength for $a = 0.03\sigma$. The hybrid-PDT approach correctly [21] accounts for its strong nonmonotonic variation, including an almost four-decade faster relaxation for the most glass-melted state which occurs at an attraction strength close to the nose of the ideal arrest boundary in Fig. 2(a). In qualitative contrast, only a hint of nonmonotonicity is observed when the projected effective force is used, which disagrees with experiment and simulation for the physical reasons discussed in depth previously [21].

We now study the mean time scale associated with the three shorter length scale dynamical processes of present interest: (a) the bond-breaking time scale τ_b, for displacing uphill on the dynamic free energy from $r = r_L$ to $x = r_L(\phi, a/\sigma, \beta\epsilon) + a$ [blue arrow in Fig. 2(b)]; (b) the decaging time scale τ_d, where $x = R^*(\phi, a/\sigma, \beta\epsilon)$ [red arrow in Fig. 2(b)]; (c) the time to move a *fixed* distance $x = 0.10\sigma$ defined as $\tau_{0.1\sigma}$ [green arrow in Fig. 2(b)] per Fig. 1. The displacement associated with (a) is the smallest, while that of (b) and (c) are comparable with their relative magnitude depending on the system state point. Since the dynamic free energy minimum at r_L defines the displacement of the transiently localized bonded and caged state, it is a natural choice for the lower limit in Eq. (3) for addressing processes (a) and (b). For process (c), we have verified our calculations of $\tau_{0.1\sigma}$ are insensitive to further reduction of the lower limit, and the reason is that "downhill" motion from $r = 0 \to r_L$ is extremely fast.

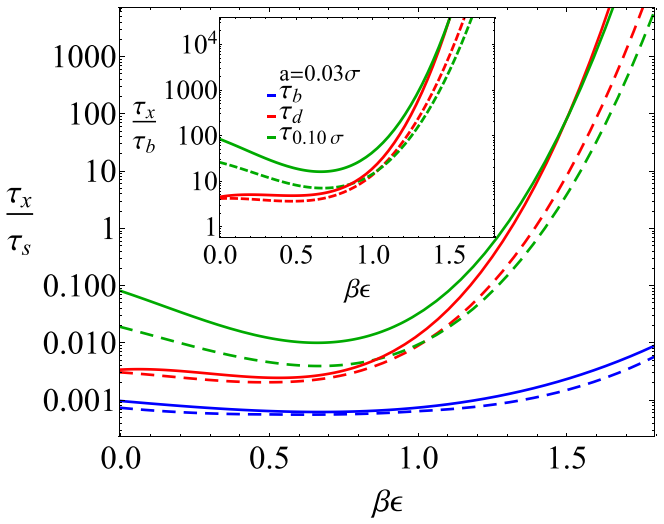

FIG. 3. Nondimensionalized bond-breaking (blue), decaging (red), and fixed distance displacement of 0.10σ (green) time scales with $a = 0.03\sigma$ for $\phi = 0.58$ (dashed) and $\phi = 0.60$ (solid) using the hybrid-PDT effective force idea. Inset: ratio of decaging (red) and fixed displacement (green) time scales to the bond-breaking time scale for the same packing fractions and attraction range.

We emphasize that the results presented below are of general interest beyond the specific ZP simulation study [6]. But in order to use those simulations to test our ideas, we note that its MSDs were largely determined at $\beta\epsilon = 0,\ 1.67,\ 5$. The latter two values differ by a factor of 3, and the middle value is close to the nose feature per Fig. 1(b). This motivates our choice of parameters: an intermediate $\beta\epsilon = 0.5$ close to the theory-predicted nose in Fig. 2(a), and a value three times larger, $\beta\epsilon = 1.5$. The baseline attraction range and packing fraction are taken to be 3% and 0.58, respectively; a few results will be shown or discussed for other choices.

The main frame of Fig. 3 presents the three time scales in a common elementary unit as a function of attraction strength corresponding to vertical trajectories in Fig. 1 that transverse the RG, F, and BRG states. The inset quantifies the degree of decoupling, defined as the ratio of the two slower time scales to the bond lifetime. Since bond breaking occurs on a much smaller length scale and is thus faster than the other two processes, decoupling is generically expected. However, its magnitude and rich evolution with system parameters cannot be guessed, and our predictions serve as a sensitive test of the microscopic physics encoded in the dynamic free energy. There are multiple notable trends in Fig. 3.

For the hybrid-PDT based theory all time scales exhibit only a weakly nonmonotonic behavior, enormously gentler than predicted [21] for the structural alpha time. This reflects the unimportance of collective elastic effects and much smaller particle displacements for in-cage processes. For attraction strengths beyond the nose in Fig. 2(a), the decaging time and $\tau_{0.1\sigma}$ are nearly the same since the corresponding displacements are close. The bond-breaking time varies much more weakly with attraction strength mainly because of the smaller displacement of this event. We also find that the

qualitative nature of the weak nonmonotonic variation of time scales, weaker dependence of the bond-breaking time compared to the other two time scales, and quantitative similarity of τ_d and $\tau_{0.1\sigma}$ beyond the nose are all independent of the precise value of (high) packing fraction and (short) attraction range. Hence, our deductions based on Fig. 3 are general. The weak nonmonotonicity in the main frame of Fig. 3 is a prediction that can be tested in future simulations that employ a finer grain variation of attraction strength.

The inset of Fig. 3 shows the decoupling ratios for the decaging and fixed displacement time scales relative to the bond-breaking time scale. Both ratios grow strongly and similarly with attraction strength in the strong bond formation regime. Mechanistic physical insight to the origin of this trend follows from examining the differences in the magnitude of the real space displacement, dynamic free energy cost, and cage restoring force for the decaging and bond-breaking events, as shown in Fig. SM2 of the SM [27]. These decoupling ratios increase very strongly (not plotted) with packing fraction. For example, at $\beta\epsilon = 1.5$ the decoupling ratio is $\sim 10^2, 10^4, 10^6$ for packing fractions (spanning the DG to BRG regimes) of 0.56, 0.58, 0.60, respectively. This large growth with modest packing fraction increase seems consistent with the evolution from a DG to BRG [6].

The analogous results to those in Fig. 3 based on the projected effective force approximation are shown in Fig. SM1 of the SM [27]. They are very different, exhibiting little change or even opposite trends with attraction strength, and do *not* seem physical. We thus conclude that an explicit treatment of attractive *forces* is essential to capture the correct physical behavior of shorter length and time scale in-cage activated processes.

The simulation [6] vertical trajectory results summarized in Table I can be compared to our calculations. States VI, VII, and VIII are close to the nose in the kinetic arrest diagram. States V, IV, and III are reached from VI, VII, and VIII by increasing attraction strength by a factor of $\sim$3 at fixed $\phi = 0.57$, 0.59, and 0.612, respectively. We map [30,31] $\phi = 0.57$ of the simulation mixture model to 0.56 in our monodisperse model; the other two states then roughly correspond to $\phi = 0.58$ and 0.60, respectively. The nose in the ideal kinetic arrest diagram for $a = 0.03\sigma$ is at $\beta\epsilon \sim 0.55$, so a factor of $\sim$3 increase in attraction strength is $\beta\epsilon = 0.55 \rightarrow 1.65$. These "calibrated" parameter choices allow us to plausibly compare theory and simulation for $\tau_{0.1\sigma}$. The results are given in Table I. We uniformly find consistent, and in some cases nearly quantitative, agreement. This seems especially significant since the overall time scale change can be as large as five decades, and the degree of variation is highly trajectory specific.

Concerning the dependence on fluid density, we recall that for pure hard spheres as $\phi = 0.56 \rightarrow 0.61$ ECNLE theory predicts [17] that the structural relaxation time grows by $\sim$9 decades. In contrast, all time scales of all faster local processes show much weaker growth, with bond-breaking times exhibiting the weakest packing fraction dependence (Fig. 3 main frame). These trends are in qualitative or semiquantitative accord with simulation [6]. For example, at high $\beta\epsilon = 1.5$, Fig. 3 shows that the bond-breaking times increase by a factor of $\sim$3, while the other two time scales associated with larger length scale displacements grow by $\sim$2 decades over the same packing fraction range. The form of the packing fraction dependence is roughly exponential, to a degree that varies nonmonotonically with attraction strength, and is largest for high attractions when bonding is strong (see Fig. SM3 of the SM [27]). As another testable prediction we find that as the attraction range increases, the rate of growth of all the time scales relative to their hard sphere fluid value decreases (see Fig. SM3 of the SM [27]).

Finally, we note that Ndong Mintsa *et al.* [32] employed simulation to study bond-breaking and diffusion time scales as a function of fluid density and attraction strength. The bond lifetime shows much weaker variation with both variables, compared to the diffusion coefficient. These findings are in qualitative accord with our present and prior [21] theoretical work.

Summary and outlook. We have employed the microscopic ECNLE plus hybrid-PDT theory to study attractive particle dynamics in ultradense fluids on smaller in-cage length and time scales where collective elasticity effects are unimportant. Our results for the decaging, bond-breaking, and fixed displacement time scales are in good accord with simulation [6] over a wide range of attraction strengths and packing fractions. This supports both the underlying spatially resolved dynamic free energy concept and the need to treat the direct effect of attractive *forces* to properly capture in-cage activated motions. Testable predictions are made for attraction ranges and packing fractions not yet simulated. Orders of magnitude decoupling of the bond-breaking time from the decaging time is predicted, which is greatly enhanced with increasing density. The present advance offers opportunities for theoretical understanding of other physical bond forming soft matter systems and the "double yielding" rheological phenomenon [7,33,34] under strong deformation in ultradense attractive colloidal suspensions.

Acknowledgment. This work was supported by DOE-BES under Grant No. DE-FG02-07ER46471 administered through the Materials Research Laboratory at UIUC.

[1] W. C. K. Poon, MRS Bull. **29**, 96 (2004).
[2] W. C. K. Poon, J. Phys.: Condens. Matter **14**, R859 (2002).
[3] K. N. Pham, A. M. Puertas, J. Bergenholtz, S. U. Egelhaaf, A. Moussaïd, P. N. Pusey, A. B. Schofield, M. E. Cates, M. Fuchs, and W. C. K. Poon, Science **296**, 104 (2002).
[4] T. Eckert and E. Bartsch, Phys. Rev. Lett. **89**, 125701 (2002).
[5] C. P. Royall, S. R. Williams, and H. Tanaka, J. Chem. Phys. **148**, 044501 (2018).
[6] E. Zaccarelli and W. C. K. Poon, Proc. Natl. Acad. Sci. USA **106**, 15203 (2009).

[7] K. N. Pham, G. Petekidis, D. Vlassopoulos, S. U. Egelhaaf, P. N. Pusey, and W. C. K. Poon, Europhys. Lett. **75**, 624 (2006).
[8] A. M. Puertas, M. Fuchs, and M. E. Cates, Phys. Rev. Lett. **88**, 098301 (2002).
[9] E. Zaccarelli, P. J. Lu, F. Ciulla, D. A. Weitz, and F. Sciortino, J. Phys.: Condens. Matter **20**, 494242 (2008).
[10] W. Gotze, *Complex Dynamics of Glass-Forming Liquids: A Mode-Coupling Theory* (Oxford University Press, New York, 2009).
[11] G. L. Hunter and E. R. Weeks, Rep. Prog. Phys. **75**, 066501 (2012).
[12] E. R. Weeks, J. C. Crocker, A. C. Levitt, A. Schofield, and D. A. Weitz, Science **287**, 627 (2000).
[13] P. Chaudhuri, L. Berthier, and W. Kob, Phys. Rev. Lett. **99**, 060604 (2007).
[14] E. J. Saltzman and K. S. Schweizer, J. Chem. Phys. **119**, 1197 (2003).
[15] K. S. Schweizer, J. Chem. Phys. **123**, 244501 (2005).
[16] S. Mirigian and K. S. Schweizer, J. Phys. Chem. Lett. **4**, 3648 (2013).
[17] S. Mirigian and K. S. Schweizer, J. Chem. Phys. **140**, 194506 (2014).
[18] S. Mirigian and K. S. Schweizer, J. Chem. Phys. **140**, 194507 (2014).
[19] S. Mirigian and K. S. Schweizer, Macromolecules **48**, 1901 (2015).
[20] S. J. Xie and K. S. Schweizer, Macromolecules **49**, 9655 (2016).
[21] A. Ghosh and K. S. Schweizer, J. Chem. Phys. **151**, 244502 (2019).
[22] Z. E. Dell and K. S. Schweizer, Phys. Rev. Lett. **115**, 205702 (2015).
[23] S. Amokrane and P. Germain, Phys. Rev. E **99**, 052120 (2019).
[24] P. Germain and S. Amokrane, Phys. Rev. E **81**, 011407 (2010).
[25] F. Sciortino, P. Tartaglia, and E. Zaccarelli, Phys. Rev. Lett. **91**, 268301 (2003).
[26] J. P. Hansen and I. R. McDonald, *Theory of Simple Liquids* (Academic, London, 1986).
[27] See Supplemental Material at http://link.aps.org/supplemental/10.1103/PhysRevE.101.060601 for some technical details of the theory and a few additional figures that support our discussions in the main text related to (i) calculation of the collective elastic barrier for any displacement, (ii) results based on the standard projected effective force approximation, (iii) the connection between displacement length scale, effective barrier, and cage restoring force for the in-cage processes which are especially relevant for the time scale decoupling effects, and (iv) calculations for how the in cage time scales depend on attractive force range and fluid packing fraction.
[28] E. J. Saltzman and K. S. Schweizer, Phys. Rev. E **77**, 051504 (2008).
[29] E. J. Saltzman, G. Yatsenko, and K. S. Schweizer, J. Phys: Condens. Matter **20**, 244129 (2008).
[30] D. R. Reichman, E. Rabani, and P. L. Geissler, J. Phys. Chem. B **109**, 14654 (2005).
[31] At fixed packing fraction, particle size polydispersity is well known to speed up dynamics. Since we employ a monodisperse model, the precise mapping of our packing fraction to that of the simulation [6] has modest uncertainty. Though not rigorous, we crudely account for this by reducing the simulation packing fractions by 0.01 in our theoretical calculations.
[32] E. Ndong Mintsa, P. Germain, and S. Amokrane, Eur. Phys. J. E **38**, 21 (2015).
[33] K. N. Pham, G. Petekidis, D. Vlassopoulos, S. U. Egelhaaf, W. C. K. Poon, and P. N. Pusey, J. Rheology **52**, 649 (2008).
[34] N. Koumakis and G. Petekidis, Soft Matter **7**, 2456 (2011).